THE JOURNAL OF BIOLOGICAL CHEMISTRY VOL. 281, NO. 47, pp. 35855–35862, November 24, 2006

Stored Ca^{2+} Depletion-induced Oligomerization of Stromal Interaction Molecule 1 (STIM1) via the EF-SAM Region

*AN INITIATION MECHANISM FOR CAPACITIVE Ca^{2+} ENTRY**

Received for publication, August 29, 2006, and in revised form, October 2, 2006 Published, JBC Papers in Press, October 3, 2006, DOI 10.1074/jbc.M608247200

Peter B. Stathopulos[‡1], Guang-Yao Li[‡], Michael J. Plevin[‡2], James B. Ames[§], and Mitsuhiko Ikura[‡3]

From the [‡]Division of Signaling Biology and Department of Medical Biophysics, Ontario Cancer Institute and University of Toronto, Toronto M5G 1L7, Ontario, Canada and the [§]Department of Chemistry, University of California, Davis, California 95616

Stromal interaction molecule 1 (STIM1) has recently been identified as a key player in store-operated Ca^{2+} entry. Endoplasmic reticulum (ER) luminal Ca^{2+} depletion results in STIM1 redistribution from ER membrane homogeneity to distinctly localized aggregates near the plasma membrane; these changes precede and are linked to cytoplasmic Ca^{2+} influx via Ca^{2+} release-activated channels (CRACs). The molecular mechanisms initiating ER STIM1 redistribution and plasma membrane CRAC activity are not well understood. We recombinantly expressed the Ca^{2+}-sensing region of STIM1 consisting of the EF-hand together with the sterile α-motif (SAM) domain (EF-SAM) to investigate its Ca^{2+}-related conformational and biochemical features. We demonstrate that Ca^{2+}-loaded EF-SAM (holo) contains high α-helicity, whereas EF-SAM in the absence of Ca^{2+} (apo) is much less compact. Accordingly, the melting temperature (T_m) of the holoform is ~25 °C higher than apoform; heat and urea-derived thermodynamic parameters indicate a Ca^{2+}-induced stabilization of 3.2 kcal mol^{-1}. We show that holoEF-SAM exists as a monomer, whereas apoEF-SAM readily forms a dimer and/or oligomer, and that oligomer to monomer transitions and vice versa are at least in part mediated by changes in surface hydrophobicity. Additionally, we find that the Ca^{2+} binding affinity of EF-SAM is relatively low with an apparent dissociation constant (K_d) of ~0.2–0.6 mM and a binding stoichiometry of 1. Our results suggest that EF-SAM actively participates in and is the likely the molecular trigger initiating STIM1 punctae formation via large conformational changes. The low Ca^{2+} affinity of EF-SAM is reconciled with the confirmed role of STIM1 as an ER Ca^{2+} sensor.

Calcium is a fundamental signaling messenger in every eukaryotic cell, regulating a multitude of diverse and kinetically distinct cellular phenomena including gene transcription, protein folding, protein degradation, apoptosis, necrosis, and exocytosis, to name a few (1). The endoplasmic reticulum (ER)[4] is a network of folded membranes that extends through the cytoplasm to the nuclear envelope of eukaryotes. The ER membranes surround an inner cavity, the lumen, that is critical to the function of the ER as a Ca^{2+} signaling organelle (2). Because vital Ca^{2+}-dependent processes are associated with the ER, it is essential that changes in luminal Ca^{2+} levels do not adversely affect these phenomena. Eukaryotes have evolved store-operated Ca^{2+} entry (SOCE), also termed capacitive Ca^{2+} entry, as a major Ca^{2+} entry pathway in electrochemically non-excitable cells (3–5). SOCE is the process whereby modest ER Ca^{2+} store depletion leads to plasma membrane (PM) Ca^{2+} release-activated channel (CRAC) activation, providing a sustained Ca^{2+} elevation in the cytoplasm from extracellular sources and ultimately refilling the ER luminal Ca^{2+} stores (6).

Until recently, the molecular link between ER Ca^{2+} efflux and extracellular influx was not known. However, interfering and small inhibiting RNA studies have independently implicated stromal interaction molecule-1 (STIM1) as the likely Ca^{2+} sensor in the ER (7, 8). This single-pass, type I transmembrane protein of 685 amino acids has been found localized on both the plasma and ER membranes (3–5). The N-terminal regions of STIM1 include a signal peptide, putative EF-hand motif, and predicted sterile α-motif (SAM) domain. The cytosolic C-terminal region consists of two coiled-coil domains, a Pro/Ser-rich region, and a Lys-rich region (supplemental Fig. 1*A*) (9–11). The putative EF-hand of STIM1 strongly aligns with the helix-loop-helix consensus sequence of this Ca^{2+} binding motif (supplemental Fig. 1*B*). The EF-hand in STIM1 is somewhat unorthodox because it is seemingly unpaired, whereas Ca^{2+} sensor proteins regularly have paired or doubly paired EF-hands (12, 13). Therefore, it is plausible that the putative SAM domain of STIM1 may serve to dimerize or oligomerize STIM1 in order to facilitate pairing of the EF-hand (3–5).

In the present work, the predicted Ca^{2+}-sensing region of human STIM1 comprising the EF-hand and SAM domain (EF-SAM) was expressed recombinantly in *Escherichia coli*. The

* This research was made possible through a Canadian Institute of Health Research (CIHR) operating grant (to M. I.). The costs of publication of this article were defrayed in part by the payment of page charges. This article must therefore be hereby marked "*advertisement*" in accordance with 18 U.S.C. Section 1734 solely to indicate this fact.

[S] The on-line version of this article (available at http://www.jbc.org) contains supplemental Fig. 1.

[1] Recipient of a Natural Sciences and Engineering Research Council of Canada postdoctoral fellowship.

[2] Recipient of a CIHR postdoctoral fellowship.

[3] Holds a Canada Research Chair in Cancer Structural Biology. To whom correspondence should be addressed: MaRS Toronto Medical Discovery Tower, Rm. 4-804, 101 College St., Toronto, Ontario M5G 1L7, Canada. Tel.: 416-581-7550; Fax: 416-581-7564; E-mail: mikura@uhnres.utoronto.ca.

[4] The abbreviations used are: ER, endoplasmic reticulum; PM, plasma membrane; SEC, size exclusion chromatography; CSI, chemical shift index; STIM1, stromal interaction molecule 1; SAM, sterile α-motif; SOCE, store-operated calcium entry; EF-SAM, EF-hand and SAM-containing region of STIM1; CRAC, Ca^{2+} release-activated channel; HSQC, heteronuclear single-quantum correlation; DLS, dynamic light scattering; MALS, multi-angle light scattering; ANS, 1-anilino-8-naphthalenesulfonate.

Supplemental Material can be found at: http://www.jbc.org/cgi/content/full/M608247200/DC1

behavior of EF-SAM was characterized biophysically in the presence and absence of Ca^{2+}. The results demonstrate that EF-SAM binds Ca^{2+} with an affinity that can be reconciled with physiological ER luminal and extracellular Ca^{2+} concentrations. The data establish that EF-SAM is monomeric when Ca^{2+}-loaded but readily forms dimers and oligomers in the Ca^{2+}-depleted state. This study provides a mechanistic perspective on recent observations made on changes in physical STIM1 distribution associated with Ca^{2+} fluctuations in cell culture.

MATERIALS AND METHODS

Cloning and Recombinant Expression of EF-SAM—Human STIM1 cDNA was from Origene Technologies, Inc. The EF-SAM region (Ser-58 to Gly-201) was subcloned into a pET-28a vector (Novagen, Inc.) and expressed with an N-terminal His_6 tag in BL21(DE3) *E. coli* cells. EF-SAM was purified under denaturing conditions using nickel-nitrilotriacetic acid resin and refolded according to the accompanying resin protocol (Qiagen, Inc.). After thrombin digestion, the protein was further purified by size exclusion chromatography (SEC). ApoEF-SAM was prepared from the holoform by dialysis *versus* 100 mM EDTA. Protein concentration was measured using $\epsilon_{280\,nm} = 1.54\ (mg\ ml^{-1})^{-1}\ cm^{-1}$. All experiments were performed in 20 mM Tris, 100 mM NaCl, pH 7.5, unless otherwise stated.

Optical Spectroscopy—Far-UV circular dichroism (CD) spectra were recorded on an Aviv CD spectrometer, model 62 DS (Aviv, Inc.). Data were collected in 1-nm increments using a 0.1-cm-path length (l) cell, 10-s averaging time, and 1-nm bandwidth. Spectra were corrected for buffer contributions. Thermal melts were acquired at a scan rate of $1\ °C\ min^{-1}$. Fluorescence measurements were made on a Shimadzu RF-5301PC fluorimeter (Shimadzu Corp.), and data were collected in 1 ml ($l = 1$ cm) or 0.1 ml ($l = 0.3$ cm) cuvettes using excitation and emission slit widths of 1.5 and 5 nm, respectively. 1-Anilino-8-naphthalenesulfonate (ANS; Sigma) data were collected in 0.1-ml cuvettes.

Thermodynamic parameters (T_m, ΔG, ΔH, ΔS, ΔC_p) were extracted from the thermal data by applying $N \leftrightarrow U$ and $N_2 \leftrightarrow 2U$ two-state equilibria as described previously (14). Parameters (C_{mid}, m-value, ΔG) were extracted from urea data according to the $N \leftrightarrow U$ equilibrium using the linear extrapolation method as described previously (15). Nonlinear curve fitting was performed in Origin (MicroCal Software, Inc.).

NMR Spectroscopy—Nuclear magnetic resonance (NMR) experiments were performed on 500 or 600 MHz Inova NMR spectrometers (Varian, Inc.) equipped with cryogenic, triple resonance probes. Sequential backbone assignments were made using ^1H-^{15}N HSQC, HNCACB, and CBCACONNH experiments (16, 17). The two- and three-dimensional spectra were processed, and resonance assignments were made using NMRPipe and XEASY, respectively (18, 19).

SEC and Light Scattering—SEC was performed on Superdex 75 or 200 10/300 GL columns (GE Healthcare). Multi-angle light scattering (MALS) measurements were performed in-line using the three-angle (45, 90, and 135°) miniDawn static light-scattering instrument with a 690-nm laser (Wyatt Technologies, Inc.). Molecular weight was calculated using ASTRA software (Wyatt Technologies, Inc.) based on Zimm plot analysis using a refractive index increment, $dn\,dc^{-1} = 0.185$ liter g^{-1} (20).

Dynamic light scattering (DLS) measurements were made on a Dynapro DLS module (Protein Solutions Inc.). The incident light was 825 nm, and the scattering angle was 90°. The average of 35 consecutive autocorrelation functions, each with a 10-s accumulation time, was employed for regularization deconvolution using the accompanying DYNAMICS software (Protein Solutions, Inc.).

Analytical Ultracentrifugation—Sedimentation equilibrium experiments were performed on an XL-A analytical ultracentrifuge (Beckman Coulter). The radial absorbance was scanned at 280 nm. Molecular weight determinations were made by global nonlinear least squares fitting of data at three different speeds using the accompanying EQASSOC software (Beckman Coulter). Partial specific volume = $0.729\ ml\ g^{-1}$ and sample density = $1.003\ g\ ml^{-1}$ were used in the calculations.

Ca^{2+} Titration Experiments—$^{45}Ca^{2+}$ binding assays were performed as described previously (21). For CD and fluorescence-based titrations, free Ca^{2+} was taken to be ≈ total Ca^{2+}, as protein concentration in these titrations was $\ll K_d$ values. All binding data were fit to the Hill equation using nonlinear least squares regression in MicroCal Origin.

Mass Spectrometry—Mass ionization spectra were recorded on an Applied Biosystem/MDS Sciex API QSTAR XL (Applied Biosystems, Inc.) in positive mode using a μESI source. Nondenaturing conditions were maintained by exchanging EF-SAM into a volatile buffer (NH_4HCO_3) containing a volatile Ca^{2+} source ($Ca(CH_3COO)_2$).

Protein Cross-linking—A final concentration of 0.2% (w/v) glutaraldehyde (Sigma) was used in each reaction. Cross-linking was allowed to proceed for 5 min at 4 °C before being stopped by the addition of SDS-PAGE loading buffer followed by boiling for 10 min. SDS-PAGE and Coomassie staining were performed using standard procedures.

RESULTS

HoloEF-SAM Is a Well Folded α-Helical Protein—The secondary structure of recombinant EF-SAM was assessed using far-UV CD. The spectrum of EF-SAM measured in the presence of Ca^{2+} (holo) was typical of an α-helical protein, with two intense minima at ~208 and 225 nm and a maximum at <200 nm (Fig. 1*A*). The relatively high intensity of the bands suggests that EF-SAM is well folded in the presence of Ca^{2+}. In the absence of Ca^{2+} (apo), the minimum at 225 nm weakened along with an observed blue shift in the 208 nm peak (*i.e.* new minimum at 204 nm) (Fig. 1*A*).

The considerable conformational differences between holo- and apoEF-SAM were confirmed using NMR. The ^1H-^{15}N HSQC spectrum acquired in the presence of Ca^{2+} was well dispersed (*i.e.* $^1H(N)$ backbone resonances ~10.3–6.5 ppm), consistent with a well folded and compact tertiary structure (Fig. 1*B*). The most downfield-shifted backbone ^1H resonance (~10.3 ppm) was assigned to the conserved glycine in the Ca^{2+}-binding loop (Gly-81), suggesting that the EF-hand chemical shift pattern in STIM1 follows the canonical EF-hand archetype (Fig. 1*B*; also see supplemental Fig. 1*B*) (22, 23). Chemical shift index (CSI) calculations (24) from standard triple resonance-

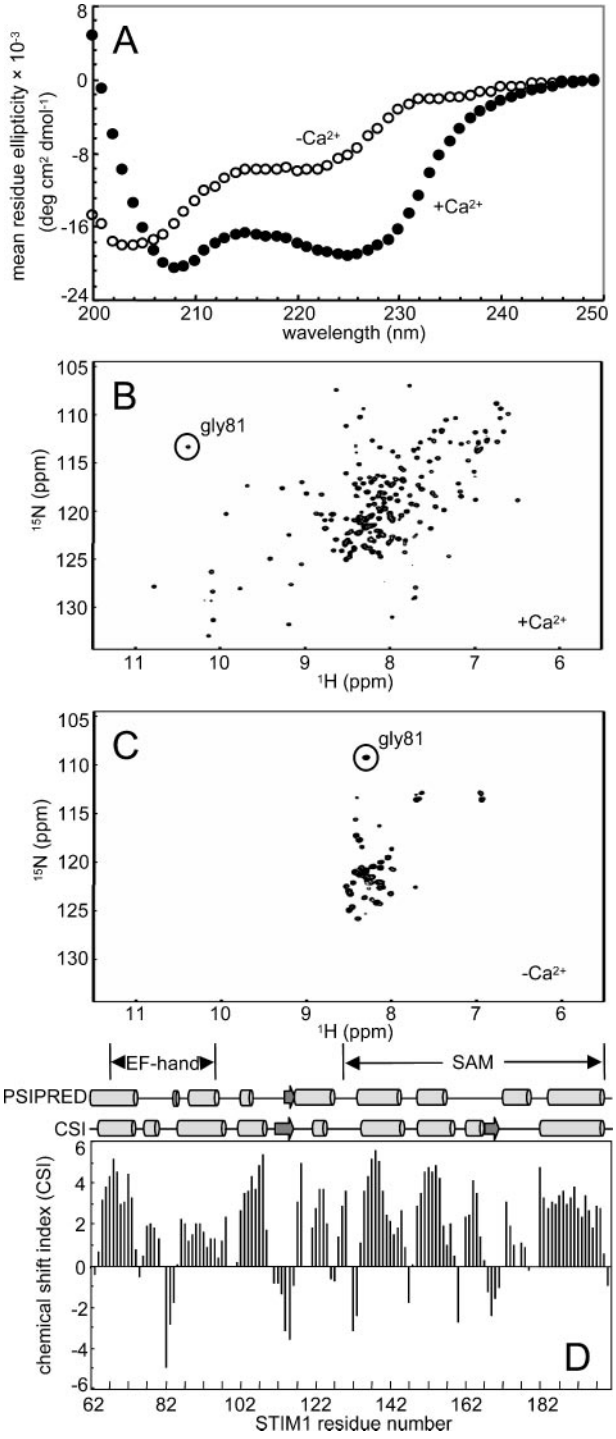

FIGURE 1. **Ca^{2+}-related structural changes in EF-SAM.** *A*, far-UV CD spectra in the presence (●) and absence (○) of Ca^{2+} at 20 °C. Protein at 0.15 mg ml^{-1} was incubated with 0.5 mM EDTA for apo. The holocurve was measured after adding 10 mM $CaCl_2$ to the aposample. *B* and *C*, ^1H-^{15}N HSQC spectra of Ca^{2+}-loaded (*B*) and -depleted (*C*) EF-SAM at 20 °C. Solution conditions were ~10 mg ml^{-1} protein with 2 mM $CaCl_2$ for holoEF-SAM and no added $CaCl_2$ for the apoform. The conserved glycine (*gly81*) in the EF-hand binding loop is indicated with a *circle*. *D*, $^{13}C^{\alpha}$–$^{13}C^{\beta}$ CSI *versus* residue number. Four or more consecutive positive CSI values indicate α-helix (*cylinders*); four or more negative values indicate a β-strand (*block arrows/arrowheads*).

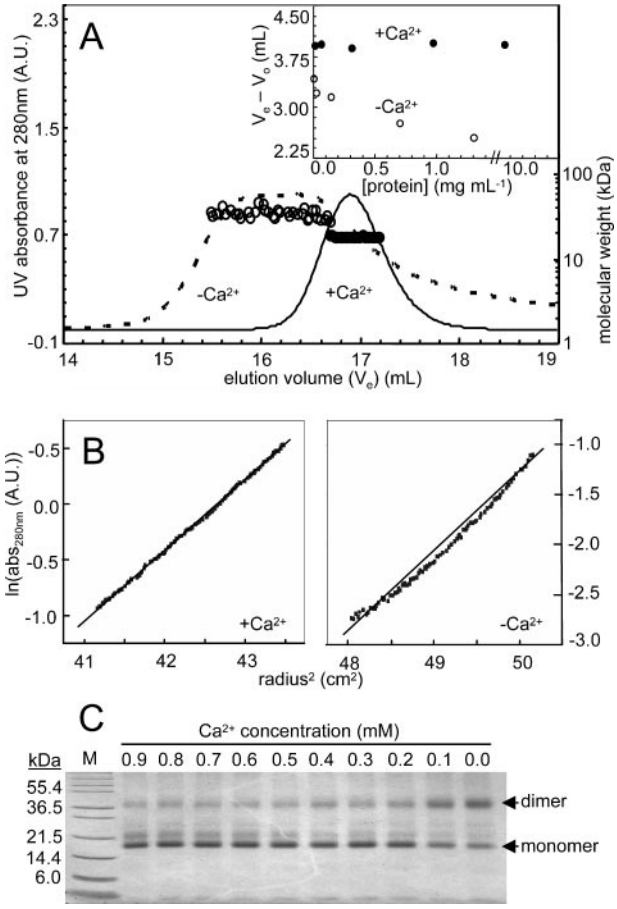

FIGURE 2. **Ca^{2+}-dependent monomerization of EF-SAM.** *A*, SEC with in-line MALS in the presence (—) and absence (– – –) of Ca^{2+} at 4 °C. Elution buffers were 2 mM $CaCl_2$ and 10 mM EDTA for holo- and apoEF-SAM, respectively. The MALS molecular weights of the holoform (●) were consistent with a monomer, whereas those of the apoform (○) were dimeric. The *inset* shows a concentration-dependent V_e for apoEF-SAM (○), which is absent for the holoform (●). *B*, sedimentation equilibrium ultracentrifugation of holo- (*left*) and apoEF-SAM (*right*) at 20 °C. Buffers contained 1 mM $CaCl_2$ and 1 mM EDTA for holo- and apoEF-SAM, respectively. Protein was at 0.32, 0.22, and 0.15 mg ml^{-1} for apo- and 0.72, 0.53, and 0.36 mg ml^{-1} for holoEF-SAM. *C*, glutaraldehyde cross-linking as a function of Ca^{2+}. Reactions were performed at 0.8 mg ml^{-1} protein, and 4 °C. 0.01 mg protein was loaded per lane.

based backbone assignments suggest that holoEF-SAM predominantly adopts α-helical secondary structure, which is in agreement with PSIPRED predictions (25) (Fig. 1*D*). The ^1H-^{15}N HSQC spectrum of apoEF-SAM was starkly different; $^1H(N)$ backbone amides had chemical shifts clustered in the ~8.5-7.5-ppm range, and the number of observable peaks decreased significantly (Fig. 1*C*). The narrow dispersion of $^1H(N)$ backbone chemical shifts indicated that apo- is considerably less folded than holoEF-SAM. The addition of Ca^{2+} to the aposample restored peak dispersion; however, the intensity of the peaks were weak relative to the holosample shown in Fig. 1*B*, likely because of slow reversibility in the aggregation of apoEF-SAM (data not shown).

HoloEF-SAM Is Monomeric—Because the majority of eukaryotic Ca^{2+} sensor proteins have paired or doubly paired EF-hands (12, 13), the molecularity of apo- and holoEF-SAM was assessed. SEC showed a single peak in the presence of excess Ca^{2+} with no evidence for changes in elution volume as a function of protein concentration (Fig. 2*A*, *inset*). SEC in-line MALS gave a Zimm plot-based molecular mass of ~18 kDa, nearly identical to the expected mass of the monomer (17.4

kDa) (Fig. 2*A*) (20). In the presence of excess EDTA, a concentration-dependent elution volume was observed (Fig. 2*A*, *inset*), and the MALS-determined molecular mass (~35 kDa) was indicative of a dimer (Fig. 2*A*). The apochromatogram showed evidence for the presence of higher order oligomeric species with considerable protein eluting in the void volume (data not shown). Ultracentrifugation sedimentation equilibrium experiments of holoEF-SAM demonstrated linear plots of ln(abs) *versus* radius^2 for all centrifugation speeds, suggesting that the sample was composed primarily of one species (Fig. 2*B*). The molecular mass, determined using global self-association analysis, was 14.8 kDa, consistent with a monomer (Fig. 2*B*). Apoprotein gave a nonlinear plot of ln(abs) *versus* radius^2 only at the highest centrifugation speed, suggesting that the sample was composed of more than one species (Fig. 2*B*). Global self-association analysis of all apoform data sets gave a molecular mass of 33.8 kDa, consistent with a dimer. The best data fits (*i.e.* lowest variance) were with the monomer-dimer-tetramer model for apoform data. Glutaraldehyde-mediated cross-linking of EF-SAM as a function of Ca^{2+} concentration was visualized by SDS-PAGE and Coomassie staining. The intensity of the monomer band increased with Ca^{2+} levels, whereas the highest dimer population was observed in the absence of Ca^{2+} (Fig. 2*C*). The molecularity experiments demonstrated that the SAM domain does not function as a dimerization motif when EF-SAM is Ca^{2+} loaded; at the same time, the apoform displays a clear tendency to form dimers and/or oligomers.

EF-SAM Binds Ca^{2+} with Low Affinity—$^{45}Ca^{2+}$ binding to EF-SAM was assessed at ambient temperature using an equilibrium ultrafiltration procedure (21). At saturation, the molar ratio of bound Ca^{2+} to EF-SAM was ~1 (Fig. 3*A*). Positive electrospray ionization mass spectrometry under native buffering conditions and in the presence of excess Ca^{2+} showed a single Ca^{2+}-related adduct attributed to Ca^{2+}- and Na^+-bound EF-SAM (*i.e.* $+40(Ca^{2+})$, $+23(Na^+)$, $-3(H^+)$), confirming the notion of a single Ca^{2+} binding site (Fig. 3*A*, *inset*). The $^{45}Ca^{2+}$ data analyzed with the Hill equation showed that binding was of low affinity (K_d ~0.6 mM) (Fig. 3*A*). The low affinity resulted in substantial data scatter and great uncertainty in the $^{45}Ca^{2+}$-fitted K_d (Fig. 3*A*; Table 1). At 20 °C, the intrinsic fluorescence emission spectra of apo- and holoEF-SAM (λ_{ex} = 280 nm) were distinct; the Ca^{2+}-loaded form had a higher fluorescence intensity and was red-shifted by ~2 nm compared with the apoform (Fig. 3*B*, *inset*). Change in fluorescence intensity as a function of Ca^{2+} levels was employed as a further probe to assessing binding affinity. The K_d derived from the Hill-fitted data was ~0.6 mM (Table 1; Fig. 3*B*). At 10 °C, where the fraction of folded apoEF-SAM was shown to be higher (see below), apparent K_d values were ~0.2 mM (Table 1; Fig. 3*B*). CD ellipticity at 208, 222, and 230 nm as a function of Ca^{2+} concentration was also used to probe affinity. Hill-based K_d values were consistent with other measurements at 20 °C (~0.5 mM) (Table 1; Fig. 3*C*). Overall, the data show that Ca^{2+} binds to EF-SAM with low affinity (sub-mM), consistent with STIM1 functioning as an ER luminal Ca^{2+} sensor.

Ca^{2+} Drastically Increases the Thermodynamic Stability of EF-SAM—The thermal stability of EF-SAM was assessed in the presence and absence of Ca^{2+} by following changes in CD ellipticity at 225 nm as a function of temperature (Fig. 4*A*). Revers-

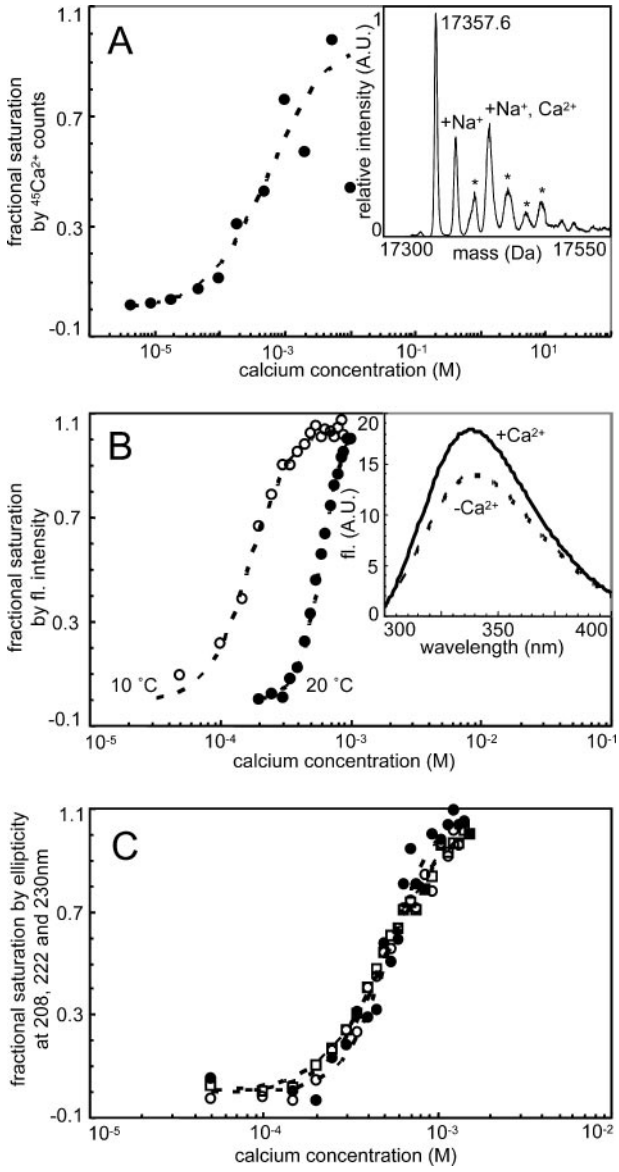

FIGURE 3. **Ca^{2+} binding curves of EF-SAM.** *A*, $^{45}Ca^{2+}$ binding to 0.87 mg ml^{-1} protein at ambient temperature. *Inset* shows the deconvoluted "native" mass spectrum of 0.64 mg ml^{-1} EF-SAM in 10 mM NH_4HCO_3, 1 mM $Ca(CH_3COO)_2$, pH 6.8. Peaks not associated with Ca^{2+} are indicated by an *asterisk*. *B*, Ca^{2+} binding monitored by changes in intrinsic fluorescence emission (λ_{ex} = 280 nm) at 10 °C (○) and 20 °C (●). Protein was at 0.03 mg ml^{-1} (20 °C) and 0.05 mg ml^{-1} (10 °C). The *inset* shows 20 °C emission spectra of apo- (– – –) and holoEF-SAM (—). *C*, Ca^{2+} binding monitored by changes in far-UV CD (208 (○), 222 (●), and 230 nm (□)) at 20 °C. Protein was at 0.15 mg ml^{-1}. *Broken lines* in *A–C* are the Hill equation fits.

TABLE 1
Apparent Ca^{2+} dissociation constants derived from the Hill equation

Probe	Temperature	K_d
	°C	mM
$^{45}Ca^{2+}$	~22[a]	0.55 ± 0.12
Fluorescence	10	0.17 ± 0.04
Fluorescence	10	0.19 ± 0.11
Fluorescence	10	0.49 ± 0.06
Fluorescence	20	0.60 ± 0.05
CD(208 nm)[b]	20	0.52 ± 0.03
CD(222 nm)[b]	20	0.51 ± 0.02
CD(230 nm)[b]	20	0.52 ± 0.02

[a] Performed at ambient temperature.
[b] Derived from 200–240-nm spectra of one titration.

ibility was ~70% when scanning just to the end of the unfolding transition. Thermodynamic analysis with a native to unfolded ($N \leftrightarrow U$, where N is native and U is unfolded) equilibrium yielded good fits to both curves (Fig. 4*A*). The temperature at which the fraction of unfolded macromolecules = 0.5 (T_m) was ~25 °C higher for holo- compared with apoEF-SAM, translating into a 3.2-kcal mol^{-1} monomer increase in Gibbs free energy of unfolding (ΔG) (Table 2). The difference in heat capacity of the protein between the folded and denatured state (ΔC_p) was considerably higher for holo- compared with apoEF-SAM, reflecting a greater cooperativity and change in solvent-accessible surface area (ΔSASA) upon unfolding (Table 2) (26).

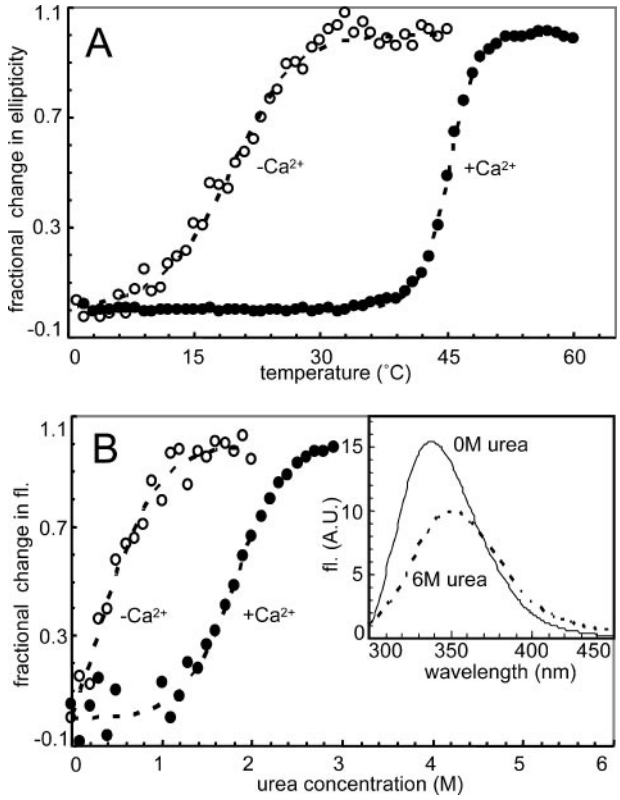

FIGURE 4. **Ca^{2+}-induced thermodynamic stabilization of EF-SAM.** *A*, thermal unfolding of EF-SAM in the presence (●) and absence of Ca^{2+} (○) monitored by changes in far-UV CD at 225 nm. Samples contained 0.30 mg ml^{-1} protein with 2 mM $CaCl_2$ and 5 mM EDTA for holo- and apoEF-SAM, respectively. *B*, urea unfolding of EF-SAM in the presence (●) and absence (○) of Ca^{2+} monitored by intrinsic fluorescence (λ_{ex} = 280 nm, λ_{em} = 330 nm) at 10 °C. The *inset* shows the emission spectra of folded and unfolded protein. Protein was at 0.0035 mg ml^{-1}, with 2.5 mM $CaCl_2$ and 5 mM EDTA for holo- and apoEF-SAM, respectively. Fits are shown as *broken lines* in both *A* and *B*.

Unlike thermal denaturation, chemical denaturation was completely reversible. Urea denaturation was monitored by following the changes in intrinsic fluorescence. Urea unfolding induced a red shift and a decrease in the intensity of the emission spectrum (λ_{ex} = 280 nm) (Fig. 4*B*, *inset*). The fluorescence of the fully folded apostate was confirmed by using 10% (v/v) glycerol. The glycerol-stabilized curve had a folded base line with emission spectra identical to apoprotein in the absence of urea and glycerol. Data were fit to the $N \leftrightarrow U$, scheme and the linear extrapolation method was used to calculate ΔG (Table 2) (15). The concentration of urea, where the fraction of unfolded macromolecules = 0.5 (C_{mid}), was significantly higher for the holo- *versus* apocurves (0.23 and 2.02 M, respectively) (Fig. 4*B*). The cooperativity of unfolding, reflected in the fitted *m*-values, was higher for holo, consistent with the ΔC_p trend (26). ΔG values were somewhat lower than those determined by thermal analysis, but both analyses (thermal and chemical) were in excellent agreement regarding the Ca^{2+}-induced stabilization (= +3.2 kcal mol^{-1} monomer).

ApoEF-SAM Reversibly Forms Oligomers—The solvent-accessible hydrophobicity of EF-SAM in the presence and absence of Ca^{2+} was probed by monitoring the extrinsic fluorescent properties of ANS (27). The emission spectrum of ANS incubated with apoEF-SAM was blue-shifted and demonstrated increased intensity compared with ANS with no protein added (Fig. 5*A*). Upon the addition of saturating concentrations of Ca^{2+}, the spectrum shifted back to longer wavelengths and displayed a decreased intensity compared with the apoform; but it remained blue-shifted and more intense than ANS alone (Fig. 5*A*). The ANS data suggest that the conformational transition that accompanies Ca^{2+} depletion includes an increase in solvent-accessible hydrophobic area.

Dynamic light scattering was employed to determine differences in propensity to oligomerization as a function of Ca^{2+}. Upon the addition of Ca^{2+}, the decays in the apoform correlation function shifted to shorter delay times, indicative of smaller hydrodynamic radii (Fig. 5*B*, *inset*). Mass-weighted regularization deconvolution results indicated that the majority of protein in the holosample had a radius of hydration consistent with monomer (*i.e.* <1.5 nm), whereas the distribution of radii in the aposample was indicative of larger dimeric/oligomeric species (Fig. 5*B*). The DLS data suggest that Ca^{2+} can induce the dissociation of oligomeric apoEF-SAM into smaller subunits.

TABLE 2

Thermodynamic parameters for apo- and holoEF-SAM

Errors for ΔG from thermal data and C_{mid} from urea data were propagated using standard propagation rules.

Protein[a]	Probe[b]	T_m	$\Delta H(T_m)$[c]	$\Delta C_p(T_m)$[d]	C_{mid}	*m*-value	ΔG (10 °C)[e]	$\Delta\Delta G$ (10 °C)[f]
		°C	kcal mol^{-1}	kcal mol^{-1} K^{-}	M	kcal mol^{-1} M^{-1}	kcal mol^{-1}	kcal mol^{-1}
$+Ca^{2+}$	Thermal	45.2 ± 0.0	122.6 ± 2.0	4.5 ± 0.3			4.5 ± 0.3	+3.2
$-Ca^{2+}$	Thermal	19.2 ± 0.2	43.0 ± 2.0	0.8 ± 0.5			1.3 ± 0.8	
$+Ca^{2+}$	Urea				1.8 ± 0.1	2.1 ± 0.2	3.7 ± 0.4	+3.2
$-Ca^{2+}$	Urea				0.3 ± 0.8	1.7 ± 0.4	0.5 ± 0.4	

[a] $+Ca^{2+}$ = excess $CaCl_2$; $-Ca^{2+}$ = excess EDTA.
[b] Thermal = CD melting curve; Urea = intrinsic fluorescence chemical denaturation curve.
[c] $\Delta H(T_m) = \Delta H$ at the melting temperature.
[d] $\Delta C_p(T_m) = \Delta C_p$ at the melting temperature.
[e] ΔG (10 °C) = ΔG at 10 °C.
[f] $\Delta\Delta G$ (10 °C) = $\Delta G_{holo} - \Delta G_{apo}$ at 10 °C.

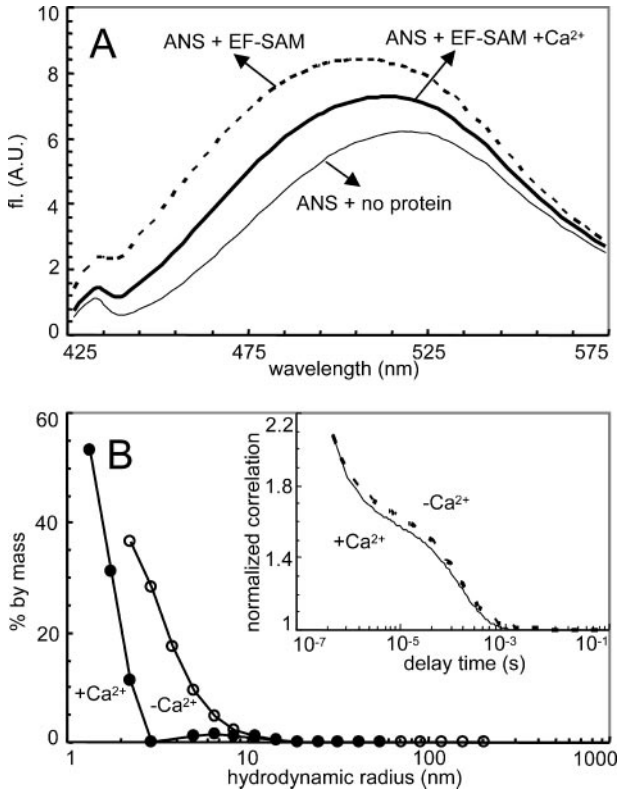

FIGURE 5. **Ca^{2+}-associated hydrophobic and oligomerization properties.** *A*, extrinsic ANS-induced fluorescence (λ_{ex} = 372 nm) in the presence (—) and absence (– – –) of Ca^{2+} at 10 °C. Protein was at 0.011 mg ml^{-1} with 0.05 mM ANS and 0.5 mM EDTA. ANS with no protein in the presence of EDTA and $CaCl_2$ gave identical spectra (—). The holoform spectrum was measured after the addition of 5 mM $CaCl_2$ to the aposample. *B*, deconvoluted DLS correlation functions in the presence (●) and absence (○) of Ca^{2+} at 15 °C. Protein was at 0.15 mg ml^{-1}, with 1 mM EDTA. Holoform data were acquired after the addition of 30 mM $CaCl_2$ to the aposample. The *lines* are to guide the eye. *Inset* shows the normalized correlation functions for apo- (– – –) and holoEF-SAM (—).

DISCUSSION

Studies have implicated STIM1 as a potent mediator of SOCE and CRAC activity (7, 28, 29). More recent experiments have identified other essential elements in these processes. For example, Orai1 is an important CRAC component that works synergistically with STIM1 to conduct Ca^{2+} into the cytoplasm from extracellular provisions (30–35). It is now thought that STIM2 redistributes with STIM1 to ER-localized aggregates that approach the PM (punctae) for CRAC regulatory purposes (36). Interactions between STIM1 and transient receptor potential channels (TRPC1) in association with SOCE also have been identified (37, 38). Nonetheless, rudimentary instigation of SOCE is related to changes in STIM1 distribution responding to ER luminal Ca^{2+} levels. The putative Ca^{2+}-sensing region of STIM1 contains a predicted EF-hand motif and SAM domain. EF-hands consist of two short α-helical segments linked through a loop region, the residues of which confer a Ca^{2+} binding site (12, 13, 39, 40). SAMs are five-helix bundle domains that often mediate protein-protein interactions via N- and C-terminal associations (41). We studied the conformational and biochemical features of EF-SAM to gain insight into the mechanisms of STIM1 Ca^{2+}-sensing initiating SOCE.

Previous experiments have shown that removing anionic residues in the predicted Ca^{2+} binding loop result in constitutive STIM1 punctae formation that is independent of ER Ca^{2+} store depletion (7, 28, 29). However, our ^1H-^{15}N HSQC data substantiated direct canonical EF-hand Ca^{2+} binding (22, 23) by revealing a downfield amide ^1H assigned to Gly-81 of the binding loop. Additionally, the CSI-assigned secondary structure ascertains the existence of two helical segments flanking each side of the Ca^{2+} binding region, also consistent with an EF-hand (42). There is considerable variability in the affinity of EF-hands for Ca^{2+}, depending on architecture ($K_d \sim 10^{-4} - 10^{-9}$ M) (12, 39). The EF-SAM binding affinities reported herein are in the same range as those for recombinantly expressed EF-hand peptides (*i.e.* $K_d = 10^{-3}$–10^{-5} M) (43). Additionally, other ER resident Ca^{2+}-binding proteins (*i.e.* calreticulin) have comparable affinity (*i.e.* $K_d = 10^{-3}$ M) (44). Free Ca^{2+} concentrations in the ER lumen of eukaryotes have been estimated at ~0.2–2 mM (44–46). Low affinity can be reconciled with these high Ca^{2+} levels and is amenable with the function of STIM1 as an ER sensor, given the myriad of Ca^{2+}-dependent processes occurring in the ER (1). Highly efficient Ca^{2+} chelation would be detrimental to these processes by requiring extremely low Ca^{2+} concentrations for STIM1 punctae formation. PM-associated STIM1 has an extracellularly directed EF-SAM region, where Ca^{2+} levels are maintained at ~1–2 mM (47). Although there is no evidence that STIM1 senses changes in extracellular Ca^{2+}, the low Ca^{2+} affinity of EF-SAM is congruent with its PM orientation.

In polypeptide terms, Ca^{2+} sensors can be defined as proteins that undergo a conformational response to the binding or dissociation of Ca^{2+}, ultimately regulating some specific function (12). The predisposition of apoEF-SAM to adopt a much less compact tertiary structure, with appreciably less α-helicity compared with holo, has been observed with other Ca^{2+} sensor proteins. For example, guanylyl cyclase-activating protein-2 and calcium-binding protein-1 attain a distinctly more compacted fold upon Ca^{2+} binding (48, 49). The Ca^{2+}-induced conformational change of EF-SAM is not localized to the EF-hand region. The ^1H-^{15}N HSQC spectra indicate a drastic global structural change upon Ca^{2+} binding or dissociation. Also, Ca^{2+} binding to the EF-hand affected the fluorescence of tryptophan residues located solely in the SAM domain, and large differences in the apo- and holoform far-UV CD as well as near-UV CD (data not shown) spectra were observed, consistent with a global change in structure. The Ca^{2+}-induced structural change to EF-SAM translates into a 3.2-kcal mol^{-1} augmentation in thermodynamic stability. This extrinsic Ca^{2+} stabilization is in the same range as other EF-hand-containing proteins such as neuronal calcium sensor-1 (+3.5 kcal mol^{-1}), tryptic C-terminal fragment of calmodulin (+3.0 kcal mol^{-1}), and tryptic N-terminal fragment of calmodulin (+3.8 kcal mol^{-1}) (50, 51).

The conformational changes accompanying Ca^{2+} depletion promote a monomer-to-oligomer transition for EF-SAM. Thermal ΔC_p and denaturant *m*-values suggest that apoEF-SAM undergoes a smaller ΔSASA (change in solvent-accessible surface area) upon unfolding. Assuming that the denatured states of apo- and holoEF-SAM are similar, native apoEF-SAM must be more solvent-accessible and less compact than native

holo. Consistent with this notion, ANS extrinsic fluorescence demonstrated that apoEF-SAM has increased surface hydrophobicity compared with holo. Increased solvent exposure of the hydrophobic area combined with decreased stability of the apoform monomers may facilitate oligomerization as a conformationally stabilizing and solvation entropy-favoring transition. It is not likely that ionic effects play a substantial role in this transition because apoprotein in high salt (*i.e.* 300 mM NaCl) forms similar dimer and oligomers (data not shown). Although it is clear that the SAM domain does not mediate homotypic interactions in the Ca^{2+}-loaded state, its role as a homodimerization motif cannot be ruled out in the apoform.

Co-overexpression of Orai1 and STIM1 without other ancillary proteins results in immense and rapid SOCE, indicating that these proteins alone are likely to be stoichiometrically linked in CRAC function (31–33, 35). This relationship, together with the contiguous proximity of the PM to punctae, argues for a cytosolic interaction between PM-resident Orai1 and ER STIM1 (7, 30, 33, 35, 38). Consistent with this notion, expression of a partial C-terminal STIM1 truncation mutant (Δ597) results in altered CRAC pharmacological, but not activation, characteristics (29). The cytoplasmic domains of STIM1 and Orai1 encode predicted coiled-coil regions (see supplemental Fig. 1*A*) (31). Coiled-coil regions are known to mediate homotypic as well as heterotypic protein interactions (52) and could facilitate PM Orai1-ER STIM1 contacts that may be involved in CRAC activation (7, 28–33, 35, 38). Despite the controversy as to whether STIM1 translocates from the ER to the PM upon store depletion, there is evidence for a PM STIM1 role in SOCE, as external application of N-terminally directed STIM1 antibody abrogates CRAC activity (29, 37). Full-length STIM1 co-immunoprecipitates with a cytoplasmic STIM1-extracellular granulocyte colony-stimulating factor receptor chimera, supporting a C-terminally mediated interaction between STIM1 molecules (10). Overexpression of the STIM1 homolog, STIM2, prevents CRAC activation upon Ca^{2+} store depletion, suggesting a regulatory role for STIM2 (36). SAM or coiled-coil regions also may help facilitate these regulatory heterotypic interactions between STIMs or with other proteins such as TRPC1 (9, 37, 53). Interestingly, the coiled-coil region of STIM1 overlaps a predicted ezrin-radixin-moesin-like region (7, 9) that may be involved in anchoring STIM1 close to the PM upon store depletion via interactions with PM phosphatidylinositol 3,4-bisphosphate (54). Our data suggest that any potential Ca^{2+} store depletion-induced molecular interactions are instigated via an EF-SAM triggering mechanism; however, the C terminus or transmembrane regions of STIM1 are likely involved in other aspects of CRAC activation or regulation and may also play important roles in punctae architecture and stability.

In conclusion, our data provide new tangible evidence that a low-affinity EF-hand exists in STIM1 and is functional for Ca^{2+} sensing in the ER lumen, where free Ca^{2+} levels are high (sub-mM). Further, the biophysical data presented here support previous single cell imaging observations in which STIM1 displays a pervasive distribution in the Ca^{2+}-loaded state, whereas it undergoes a high density, aggregate formation on the ER membrane upon depletion. Our results further demonstrate that EF-SAM alone can promote a monomer-to-oligomer transition upon Ca^{2+} release from the EF-hand motif and that exposed hydrophobic surfaces in the EF-SAM domain actively participate in self-association of STIM1. These data underscore the significance of EF-SAM in the homotypic association mechanism of STIM1 upon Ca^{2+} depletion from the ER, which leads to activation of store-operated Ca^{2+} channels on the PM. Our data support a conformationally linked model for the control of SOCE (Fig. 6). When Ca^{2+} stores are filled, the majority of STIM1 is monomeric and is evenly distributed throughout the ER and PM. Upon Ca^{2+} store depletion, a large conformational change occurs in EF-SAM, increasing hydrophobicity and promoting ER STIM1 association as a stabilizing and solvation entropy-favoring mechanism. Oligomerized STIM1 ultimately form or add to ER punctae linking STIM1 with PM Orai1, a major component of CRAC activity. Ca^{2+} store repletion results in STIM1 disaggregation and the halting of SOCE. Further structural studies are required to elucidate a more defined picture of STIM1 action in the control of SOCE.

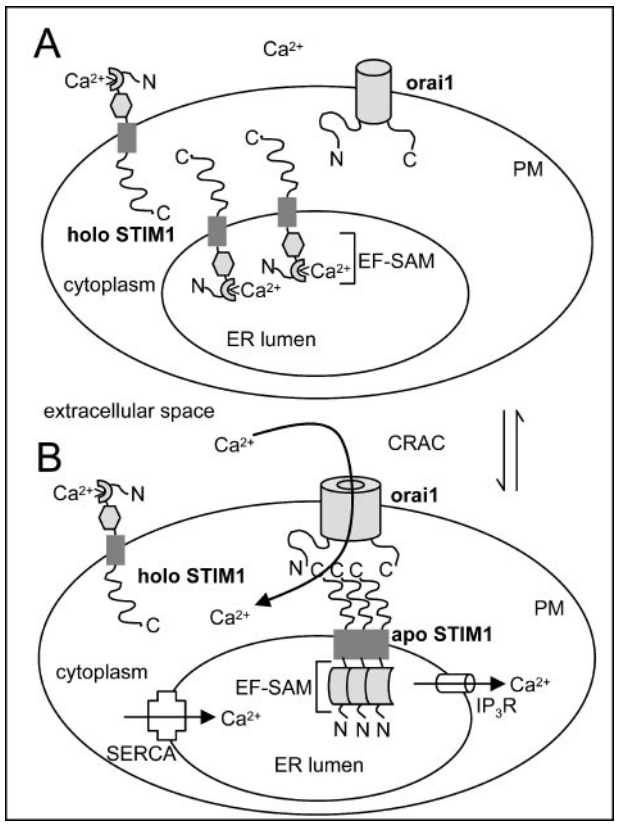

FIGURE 6. **Ca^{2+}-sensing STIM1 model of initiating SOCE in a resting cell.** *A*, at rest, holoSTIM1 exists as a monomer on the ER and PM. Inactive Orai1 is present on the plasma membrane. *B*, upon luminal Ca^{2+} store depletion due to IP_3 receptor (IP_3R) activity, Ca^{2+} dissociates from ER STIM1, resulting in a large EF-SAM structural transition. This conformational change initiates ER STIM1 homotypic associations. The localization of the STIM1 oligomers in punctae activates Orai1-mediated cytoplasmic Ca^{2+} entry. CRAC activity provides a sustained cytoplasmic Ca^{2+} increase. Sarco/endoplasmic reticulum Ca^{2+} ATPase (*SERCA*) pumps refill ER Ca^{2+} stores, and increased luminal Ca^{2+} levels induce disaggregation of STIM1, halting CRAC activity.

REFERENCES

1. Berridge, M. J., Bootman, M. D., and Roderick, H. L. (2003) *Nat. Rev. Mol. Cell Biol.* **4,** 517–529
2. Berridge, M. J. (2002) *Cell Calcium* **32,** 235–249

3. Marchant, J. S. (2005) *Curr. Biol.* **15,** R493–R495
4. Putney, J. W., Jr. (2005) *J. Cell Biol.* **169,** 381–382
5. Draber, P., and Draberova, L. (2005) *Trends Immunol.* **26,** 621–624
6. Putney, J. W., Jr. (1986) *Cell Calcium* **7,** 1–12
7. Liou, J., Kim, M. L., Heo, W. D., Jones, J. T., Myers, J. W., Ferrell, J. E., Jr., and Meyer, T. (2005) *Curr. Biol.* **15,** 1235–1241
8. Roos, J., DiGregorio, P. J., Yeromin, A. V., Ohlsen, K., Lioudyno, M., Zhang, S., Safrina, O., Kozak, J. A., Wagner, S. L., Cahalan, M. D., Velicelebi, G., and Stauderman, K. A. (2005) *J. Cell Biol.* **169,** 435–445
9. Williams, R. T., Manji, S. S., Parker, N. J., Hancock, M. S., Van Stekelenburg, L., Eid, J. P., Senior, P. V., Kazenwadel, J. S., Shandala, T., Saint, R., Smith, P. J., and Dziadek, M. A. (2001) *Biochem. J.* **357,** 673–685
10. Williams, R. T., Senior, P. V., Van Stekelenburg, L., Layton, J. E., Smith, P. J., and Dziadek, M. A. (2002) *Biochim. Biophys. Acta* **1596,** 131–137
11. Manji, S. S., Parker, N. J., Williams, R. T., van Stekelenburg, L., Pearson, R. B., Dziadek, M., and Smith, P. J. (2000) *Biochim. Biophys. Acta* **1481,** 147–155
12. Ikura, M. (1996) *Trends Biochem. Sci.* **21,** 14–17
13. Nelson, M. R., and Chazin, W. J. (1998) *Biometals* **11,** 297–318
14. Marky, L. A., and Breslauer, K. J. (1987) *Biopolymers* **26,** 1601–1620
15. Pace, C. N. (1986) *Methods Enzymol.* **131,** 266–280
16. Grzesiek, S., and Bax, A. (1993) *J. Biomol. NMR* **3,** 185–204
17. Wang, A. C., Lodi, P. J., Qin, J., Vuister, G. W., Gronenborn, A. M., and Clore, G. M. (1994) *J. Magn. Reson. B* **105,** 196–198
18. Delaglio, F., Grzesiek, S., Vuister, G. W., Zhu, G., Pfeifer, J., and Bax, A. (1995) *J. Biomol. NMR* **6,** 277–293
19. Bartels, C., Xia, T., Billeter, M., Guntert, P., and Wuthrich, K. (1995) *J. Biomol. NMR* **6,** 1–10
20. Wyatt, P. J. (1993) *Anal. Chim. Acta* **272,** 1–40
21. Ames, J. B., Hendricks, K. B., Strahl, T., Huttner, I. G., Hamasaki, N., and Thorner, J. (2000) *Biochemistry* **39,** 12149–12161
22. Ikura, M., Minowa, O., Yazawa, M., Yagi, K., and Hikichi, K. (1987) *FEBS Lett.* **219,** 17–21
23. Ikura, M., Kay, L. E., and Bax, A. (1990) *Biochemistry* **29,** 4659–4667
24. Wishart, D. S., and Sykes, B. D. (1994) *J. Biomol. NMR* **4,** 171–180
25. McGuffin, L. J., Bryson, K., and Jones, D. T. (2000) *Bioinformatics* (*Oxf.*) **16,** 404–405
26. Myers, J. K., Pace, C. N., and Scholtz, J. M. (1995) *Protein Sci.* **4,** 2138–2148
27. Stryer, L. (1965) *J. Mol. Biol.* **13,** 482–495
28. Zhang, S. L., Yu, Y., Roos, J., Kozak, J. A., Deerinck, T. J., Ellisman, M. H., Stauderman, K. A., and Cahalan, M. D. (2005) *Nature* **437,** 902–905
29. Spassova, M. A., Soboloff, J., He, L. P., Xu, W., Dziadek, M. A., and Gill, D. L. (2006) *Proc. Natl. Acad. Sci. U. S. A.* **103,** 4040–4045
30. Vig, M., Peinelt, C., Beck, A., Koomoa, D. L., Rabah, D., Koblan-Huberson, M., Kraft, S., Turner, H., Fleig, A., Penner, R., and Kinet, J. P. (2006) *Science* **312,** 1220–1223
31. Zhang, S. L., Yeromin, A. V., Zhang, X. H., Yu, Y., Safrina, O., Penna, A., Roos, J., Stauderman, K. A., and Cahalan, M. D. (2006) *Proc. Natl. Acad. Sci. U. S. A.* **103,** 9357–9362
32. Soboloff, J., Spassova, M. A., Tang, X. D., Hewavitharana, T., Xu, W., and Gill, D. L. (2006) *J. Biol. Chem.* **281,** 20661–20665
33. Peinelt, C., Vig, M., Koomoa, D. L., Beck, A., Nadler, M. J., Koblan-Huberson, M., Lis, A., Fleig, A., Penner, R., and Kinet, J. P. (2006) *Nat Cell Biol.* **8,** 771–773
34. Feske, S., Gwack, Y., Prakriya, M., Srikanth, S., Puppel, S. H., Tanasa, B., Hogan, P. G., Lewis, R. S., Daly, M., and Rao, A. (2006) *Nature* **441,** 179–185
35. Mercer, J. C., Dehaven, W. I., Smyth, J. T., Wedel, B., Boyles, R. R., Bird, G. S., and Putney, J. W., Jr. (2006) *J. Biol. Chem.* **281,** 24979–24990
36. Soboloff, J., Spassova, M. A., Hewavitharana, T., He, L. P., Xu, W., Johnstone, L. S., Dziadek, M. A., and Gill, D. L. (2006) *Curr. Biol.* **16,** 1465–1470
37. Lopez, J. J., Salido, G. M., Pariente, J. A., and Rosado, J. A. (2006) *J. Biol. Chem.* **281,** 28254–28264
38. Huang, G. N., Zeng, W., Kim, J. Y., Yuan, J. P., Han, L., Muallem, S., and Worley, P. F. (2006) *Nat. Cell Biol.* **8,** 1003–1010
39. Linse, S., and Forsen, S. (1995) *Adv. Second Messenger Phosphoprotein Res.* **30,** 89–151
40. Lewit-Bentley, A., and Rety, S. (2000) *Curr. Opin. Struct. Biol.* **10,** 637–643
41. Stapleton, D., Balan, I., Pawson, T., and Sicheri, F. (1999) *Nat. Struct. Biol.* **6,** 44–49
42. Kretsinger, R. H., and Nockolds, C. E. (1973) *J. Biol. Chem.* **248,** 3313–3326
43. Julenius, K., Robblee, J., Thulin, E., Finn, B. E., Fairman, R., and Linse, S. (2002) *Proteins* **47,** 323–333
44. Fasolato, C., Pizzo, P., and Pozzan, T. (1998) *Mol. Biol. Cell* **9,** 1513–1522
45. Barrero, M. J., Montero, M., and Alvarez, J. (1997) *J. Biol. Chem.* **272,** 27694–27699
46. Demaurex, N., and Frieden, M. (2003) *Cell Calcium* **34,** 109–119
47. Thomas, A. P. (2000) *Nat. Cell Biol.* **2,** E126—E127
48. Wingard, J. N., Chan, J., Bosanac, I., Haeseleer, F., Palczewski, K., Ikura, M., and Ames, J. B. (2005) *J. Biol. Chem.* **280,** 37461–37470
49. Ames, J. B., Dizhoor, A. M., Ikura, M., Palczewski, K., and Stryer, L. (1999) *J. Biol. Chem.* **274,** 19329–19337
50. Muralidhar, D., Jobby, M. K., Krishnan, K., Annapurna, V., Chary, K. V., Jeromin, A., and Sharma, Y. (2005) *J. Biol. Chem.* **280,** 15569–15578
51. Masino, L., Martin, S. R., and Bayley, P. M. (2000) *Protein Sci.* **9,** 1519–1529
52. Burkhard, P., Stetefeld, J., and Strelkov, S. V. (2001) *Trends Cell Biol.* **11,** 82–88
53. Oritani, K., and Kincade, P. W. (1996) *J. Cell Biol.* **134,** 771–782
54. Hoeflich, K. P., Tsukita, S., Hicks, L., Kay, C. M., and Ikura, M. (2003) *Biochemistry* **42,** 11634–11641